

1 Plate interaction in the NE Caribbean subduction zone 2 from continuous GPS observations

3 Uri S. ten Brink¹ and Alberto M. López-Venegas²

4 Received 23 February 2012; revised 19 April 2012; accepted 21 April 2012; published XX Month 2012.

5 [1] Kinematic similarities between the Sumatra and Puerto
6 Rico Trenches highlight the potential for a mega-earthquake
7 along the Puerto Rico Trench and the generation of local and
8 trans-Atlantic tsunamis. We used the horizontal components
9 of continuous GPS (cGPS) measurements from 10 sites on
10 NE Caribbean islands to evaluate strain accumulation along
11 the North American (NA) – Caribbean (CA) plate boundary.
12 These sites move westward and slightly northward relative
13 to CA interior at rates ≤ 2.5 mm/y. Provided this motion
14 originates in the subduction interface, the northward motion
15 suggests little or no trench-perpendicular thrust accumula-
16 tion and may in fact indicate divergence north of Puerto
17 Rico, where abnormal subsidence, bathymetry, and gravity
18 are observed. The Puerto Rico Trench, thus, appears unable
19 to generate mega-earthquakes, but damaging smaller earth-
20 quakes cannot be discounted. The westward motion, char-
21 acterized by decreasing rate with distance from the trench, is
22 probably due to eastward motion of CA plate impeded at the
23 plate boundary by the Bahamas platform. Two additional
24 cGPS sites in Mona Passage and SW Puerto Rico move to
25 the SW similar to Hispaniola and unlike the other 10 sites.
26 That motion relative to the rest of Puerto Rico may have
27 given rise to seismicity and normal faults in Mona Rift,
28 Mona Passage, and SW Puerto Rico. **Citation:** ten Brink,
29 U. S., and A. M. López-Venegas (2012), Plate interaction in the
30 NE Caribbean subduction zone from continuous GPS observations,
31 *Geophys. Res. Lett.*, 39, LXXXXX, doi:10.1029/2012GL051485.

32 1. Introduction

33 [2] Driven by plate motion, elastic strain accumulates in
34 locked parts of the interface between a subducting plate and
35 an overlying plate. This strain is released when the interface
36 ruptures during an earthquake. Therefore the rate and loca-
37 tion of elastic strain accumulation are of great interest for
38 earthquake hazard mitigation and for understanding earth-
39 quake physics. Approaches to estimating the rate and loca-
40 tion of elastic strain accumulation at subduction zones
41 include measuring the rates of vertical and horizontal
42 deformations landward of the subduction zone [Savage,
43 1983] using tide gauges, leveling, paleo-shoreline markers,

and most commonly Global Positioning System (GPS) 44
geodesy [e.g., Prawirodirdjo *et al.*, 1997]. 45

[3] The Puerto Rico Trench is an 800-km-long curved 46
subduction zone that wraps around the NE corner of the 47
Caribbean (CA) plate (Figure 1). According to a mix of GPS 48
and geological data, the North American (NA) plate sub- 49
ducts under the CA plate at a rate of 20.0 ± 0.4 mm/y along 50
an azimuth of $254 \pm 1^\circ$ [DeMets *et al.*, 2010]. Subduction is 51
thus highly oblique ($\geq 10^\circ$) to the NA-CA plate boundary, 52
similar to that along Sumatra subduction zone. Following 53
the 2004 Sumatra earthquake and tsunami, concern grew 54
that the Puerto Rico Trench might be capable of producing a 55
similar mega-earthquake, which could cause severe 56
destruction by ground shaking, tsunamis striking nearby 57
islands, as well as transoceanic tsunamis that could affect the 58
U.S. East Coast [Geist and Parsons, 2009] and Europe. 59
There is no clear historical or instrumental record for large 60
earthquakes along the NE Caribbean subduction zone except 61
for 20th century earthquakes north of the Dominican 62
Republic and Mona Passage (Figure 1) [ten Brink *et al.*, 63
2011]. Tsunami deposits dated at 1650–1800 A.D. were 64
found on Anegada, British Virgin Islands, but their source is 65
presently debated [Atwater *et al.*, 2012]. 66

[4] To evaluate the seismic potential of the Puerto Rico 67
Trench, we analyze the velocity field recorded by 13 con- 68
tinuous GPS (cGPS) stations in the Lesser Antilles, the 69
British and U.S. Virgin Islands, and Puerto Rico (Figure 1 70
and Table S1 in the auxiliary material), and we model 71
these data using an elastic backslip model [Savage, 1983].¹ 72
The backslip model assumes that a down-dip portion of the 73
subduction interface is fully or partially locked during the 74
interseismic period, causing the downgoing slab to drag the 75
overlying forearc and arc in the direction of subduction. 76
Locking is estimated by imposing motion in the direction of 77
subduction on the bottom of the upper plate and comparing 78
the calculated velocities at the GPS sites to the GPS obser- 79
vations. This approach was taken in other subduction zones 80
around the world [Dixon, 1993; Norabuena *et al.*, 1998; 81
Hashimoto *et al.*, 2009]. 82

[5] Manaker *et al.* [2008] divided the NE Caribbean into 83
rigid blocks and simultaneously inverted for elastic strain 84
accumulation on the plate boundary and on block boundary 85
faults. Their goal was to estimate velocities along the major 86
strike-slip fault zones traversing Hispaniola, where they had 87
dense coverage of campaign GPS data. We elected to focus 88
on the subduction interface, because GPS velocities in 89
Puerto Rico, the Virgin Islands, and St. Maarten decrease 90
gradually with distance from the plate boundary (Figure 1b), 91
which implies continuous deformation of the upper plate. 92

¹Woods Hole Science Center, U.S. Geological Survey, Woods Hole, Massachusetts, USA.

²Department of Geology, University of Puerto Rico, Mayagüez, Puerto Rico.

Corresponding author: U. S. ten Brink, Woods Hole Science Center, U.S. Geological Survey, 384 Woods Hole Rd., Woods Hole, MA 02543-1598, USA. (utenbrink@usgs.gov)

This paper is not subject to U.S. copyright.
Published in 2012 by the American Geophysical Union.

¹Auxiliary materials are available in the HTML. doi:10.1029/2012GL051485.

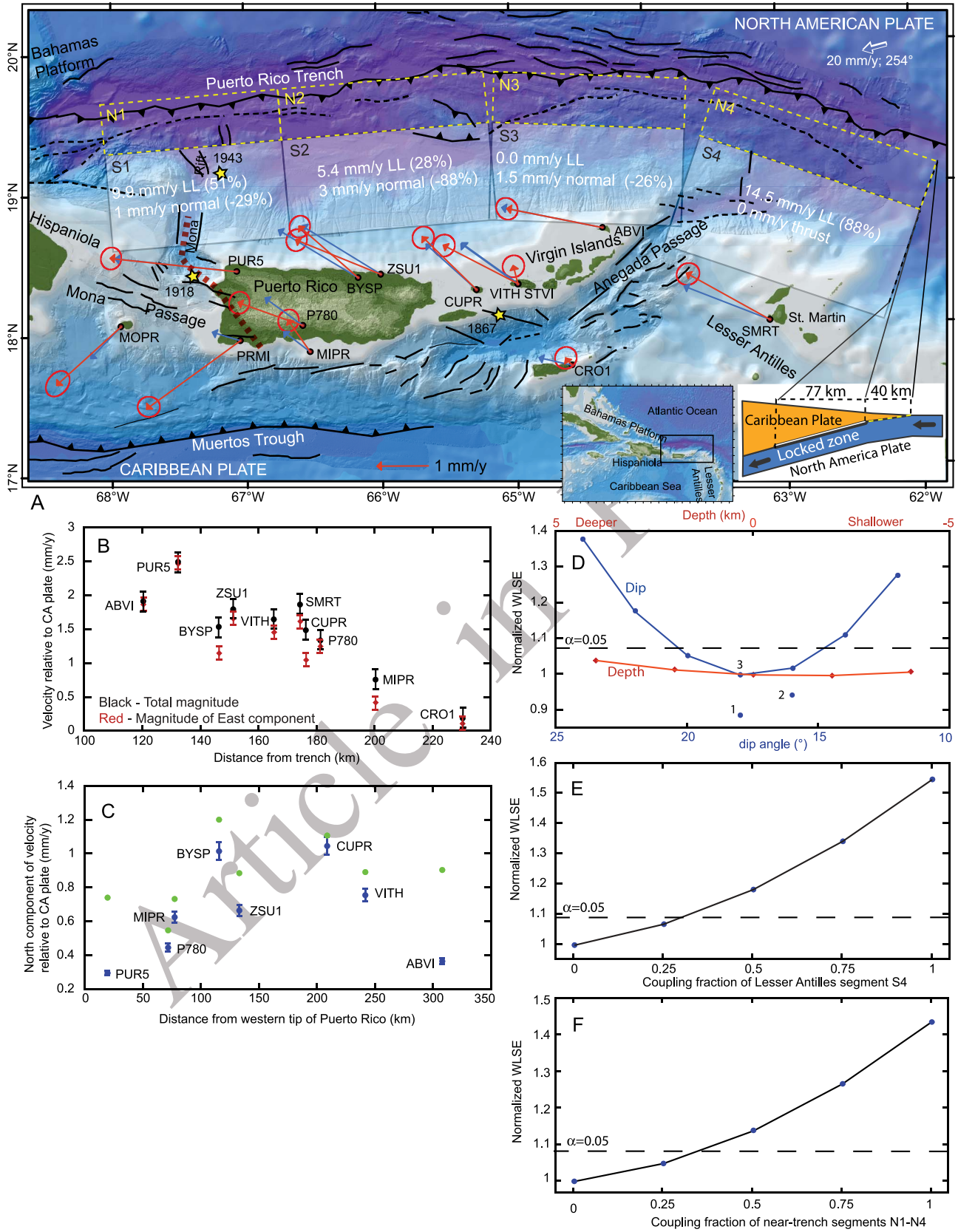


Figure 1

93 Our goal is also different, to evaluate the separate compo-
 94 nents of stress loading at the subduction interface from the
 95 observed GPS velocities on the upper plate.

96 2. Data

97 [6] Data from 13 continuously operated GPS stations in the
 98 NE Caribbean were obtained from the UNAVCO archive for
 99 a period of 2.75–5 years ending in August 2011 at sampling
 100 rates of 10, 15 or 30 s with only a few periods of interruption.
 101 Although campaign GPS data were collected in this region
 102 during the late 1990s [Jansma *et al.*, 2000; Jansma and
 103 Mattioli, 2005], this dataset is not freely available. The data
 104 were processed and analyzed using GIPSY-OASIS II release
 105 version 6 [Zumberge *et al.*, 1997] and precise clocks and
 106 orbits from NASA-JPL (see auxiliary material for more
 107 details). The data were referenced to the International Ter-
 108 restrial Reference Frame 2008 (ITRF08) frame, and then
 109 transformed to both NA and CA reference frames (Table S2)
 110 with an updated version of the NA and CA ITRF08 Euler
 111 poles (C. DeMets, personal communication, 2011).

112 [7] The cGPS data do not show evidence for transient
 113 deformation associated with slow-slip events (Figure S1)
 114 despite abundant swarms north of Puerto Rico and the Vir-
 115 gin Islands (PRVI) since March 2007. Only three $M > 7$
 116 earthquakes occurred within the network region in the past
 117 200 years, the last one in 1943 (Figure 1) [ten Brink *et al.*,
 118 2011], thus the contribution to the velocity field from post-
 119 seismic slip is likely negligible.

120 [8] In the next section we model 10 of the 13 GPS sites.
 121 Velocities of 9 sites from St. Maarten to western Puerto Rico
 122 range between 0.8 mm/yr to 2.5 mm/yr toward the NW in a
 123 CA reference frame (Figure 1 and Table S1). The 10th site,
 124 CRO1, is almost stationary. Three sites were not modeled.

STVI is located only 650 m away from VITH but has a very
 different velocity. We preferred to model VITH rather than
 STVI for two reasons: (1) STVI has been in operation for half
 the time period of VITH, and (2) VITH and CUPR have
 similar velocities. Two sites in the SW part of the network
 (MOPR and PRMI) have very different velocity vectors from
 the rest of the network and are not included in the models.
 These sites likely reflect real motion and not monument
 noise, because their velocity vectors are similar to each other
 (MOPR: 1.7 mm/y, 228°; PRMI: 2.3 mm/y, 235°) and to
 those in easternmost Hispaniola [Calais *et al.*, 2010]. Geo-
 logical interpretation of this SW motion is discussed later.

3. Models

[9] We model the interseismic strain accumulation using
Coulomb3.1 elastic half-space model [Lin and Stein, 2004;
 Toda *et al.*, 2005]. The seismogenic zone was divided into 4
 segments, S1–S4 (Table S3, and semi-transparent rectangles
 in Figure 1) to fit the curved plate boundary and the con-
 tributions from all the segments were summed for each site.
 The segments extend beyond the GPS sites to ensure that the
 calculated vectors are not affected by edge effects. The
 geometry of the subduction zone in this region is poorly
 known because of the paucity of interplate earthquakes and
 the lack of detailed seismic refraction profiles across the
 forearc and the arc. Consequently, the number of model
 parameters, $k = 28$ (4 segments each having 2 location
 points, updip and downdip depths, dip, and 2 backslip vec-
 tors) exceeds the number of observations ($j = 20$). Our
 starting model placed the seismogenic zone (i.e., the zone of
 coupling) in the forearc beginning ~ 40 km from the trench
 with up-dip and down-dip limits of 10 km and 35 km,
 respectively, and a downdip width of 80 km. Model fit was

Figure 1. (a) Shaded and colored bathymetry of the NE Caribbean. See inset for location. Arrows are observed (red) and calculated (blue) velocities relative to CA plate reference with their error ellipse (Table S1). Semi-transparent rectangles S1–S4 are the locations of surface projections of patches on which backslip was applied. Values of trench-parallel and perpendicular components of the backslip and their percentage of the respective plate convergence components are given for the preferred model. Yellow-dashed rectangles N1–N4 – Locations of 40-km-wide modeled patches close to the trench with dip slip component, discussed in the text. Cross-section in inset shows model geometry. Barbed lines, dashed lines, and solid lines – thrust, strike-slip, and normal faults, respectively. Dashed red line – interpreted boundary between Hispaniola-Mona Passage region, which moves to the SW, and PRVI, which moves to the NW, in a CA plate reference. Yellow stars – Large ($M > 7$) historical earthquakes and the year they occurred. (b) Observed total velocity magnitude (black dots) and the East component of the velocity (red dots) of the 10 modeled cGPS sites as a function of distance of sites from the trench. Black and red error bars – Average radii of error ellipses, and the radii of minor axes of the error ellipses, respectively (see Table S1). (c) Plot to test possible counter-clockwise rotation of PRVI. Blue dots – Observed N-component of velocity of 8 cGPS sites as a function of distance of sites east from western tip of Puerto Rico. Sites SMRT and CRO1 were not plotted because they are outside the proposed rotated block [Manaker *et al.*, 2008]. Green dots – Residual N-velocity components after applying a model with trench-perpendicular convergent backslip with 30% locking on segments S1–S3 (see text for further discussion). (d) Variations in model fit as a function of varying slab depth (red line) and dip (blue line). All segments were changed simultaneously. Model fit is described by weighted least square estimator (WLSE, see text) and normalized to fit of model marked 3, with parameters described in text. Models above dashed line are statistically different than model 3 at significance level $\alpha = 0.05$. Model marked 2 – same as model 3 except for uniform dip of 16° and down-dip width of 90 km. Model marked 1 – best-fit model with geometry and slip parameters shown in Figure 1a. (e) Model 1 with SMRT excluded to test how well the other GPS sites constrain slip parameters on segment S4 (Lesser Antilles). Trench-perpendicular thrust was imposed on that segment at the rate predicted by plate motion (Table S3) multiplied by varying coupling fraction. Curve shows fit of these models normalized to fit of model 1 and their statistical significance (dashed line). (f) Test of sensitivity of the geodetic network to possible near-trench thrust slip accumulation. Trench-perpendicular slip was imposed on rectangles N1–N4 in Figure 1a at a fraction of the rates predicted by plate motion (Table S3). The coupling fraction was varied from 0 to 1 and the model fits were normalized to model 1 with no coupling on N1–N4. Models above dashed line are statistically different than model 1 at $\alpha = 0.05$.

157 evaluated by the minimization of the least square estimate
158 (WLSE)

$$WLSE(k) = \sum_{j=1}^{20} \left(\frac{Y_j - m_j(k)}{\sigma_j^2} \right)^2$$

159 where, Y_j and $m_j(k)$ are the observations and model predic-
160 tions, $j = 1, 2, \dots, 20$ are the N or E component of the 10 GPS
161 sites, which are assumed to be mutually independent, and σ^2
162 are variances in the observations, which include both the
163 uncertainty of measurement and the uncertainty in the CA
164 Euler vector. An acceptable model also had to qualitatively
165 display a normal distribution of $(Y_j - m_j(k))$.

166 [10] Once an approximate set of backslip displacement
167 parameters was found, we varied the dip and depth of the
168 seismogenic zone and occasionally adjusted the backslip to
169 achieve a better fit. Our best-fit model (WLSE = 23.88,
170 marked as 1 in Figure 1d; slip parameters shown in Figure 1)
171 comprises 3 segments north of PRVI (S1–S3) with an 80-km-
172 wide seismogenic zone and a dip of 18° toward the south.
173 Segment 4 (S4 - Lesser Antilles) has a 90-km-wide seismo-
174 genic zone with a dip of 16° . A wider seismogenic zone with
175 a gentler (16°) slope off the Lesser Antilles than north of
176 PRVI, is compatible with the larger distance between the
177 trench and the arc at this location and with a published cross-
178 section from gravity modeling [Westbrook and McCann,
179 1986]. Slightly less favorable models are ones where all
180 4 segments have a dip of 16° and a uniform down-dip width
181 of 90 km (WLSE = 25.36) and a model with a dip of 18° and
182 a uniform down-dip width of 80 km (WLSE = 26.92)
183 (marked 2 and 3 in Figure 1d).

184 [11] A modified likelihood ratio statistic was applied that
185 investigates model sensitivity to varying one parameter of
186 interest, β , at a time, and comparing WLSE with that of a
187 reference model, β_0 . Models with $\beta \neq \beta_0$ can be rejected at
188 $\alpha = 0.05$ significance level, if Δ exceeds the upper α
189 quantile of the χ^2 distribution with 1 degree of freedom.

$$\Delta = 2(WLSE(k(\beta_0)) - WLSE(k))$$

189 Figure 1d shows an example where models with different
190 depths and constant dips were compared to the model
191 marked 3 described above. Models with depths within 10–
192 35 km \pm 4 km and dips within $18^\circ \pm 3^\circ$ could not be
193 rejected at $\alpha = 0.05$, and are therefore as statistically valid as
194 model 3.

195 [12] The best-fit model requires backslip in an opposite
196 direction to subduction north of PRVI, namely, trench-
197 perpendicular divergence rather than the expected conver-
198 gence. A model without divergence on S1–S3 can be
199 rejected at $\alpha = 0.001$. The absence of trench-perpendicular
200 convergence seaward of the network is unusual considering
201 that oblique subduction zones such as Sumatra show a
202 subduction-directed component [Prawirodirdjo *et al.*, 1997].
203 In contrast, 6 of our cGPS sites have a trenchward compo-
204 nent $>0.6 \pm 0.2$ mm/y, 2 of which are $>1 \pm 0.2$ mm/y
205 (Figure 1c and Table S1).

206 [13] No divergence or convergence is modeled on S4, but
207 it could be argued that modeled backslip for this segment is
208 constrained by only one site, SMRT. To test this argument,
209 we imposed on S4 the expected trench-perpendicular con-
210 vergence component from relative plate motion with various
211 percentage of locking and examined the fit to the other 9

cGPS sites (i.e., without SMRT). The fit degrades rapidly
212 with increasing coupling on S4, but trench-perpendicular
213 locking of $<30\%$ on this segment (<3.2 mm/y) could not be
214 rejected $\alpha = 0.05$ (Figure 1e). The presence of shallow
215 forearc thrust earthquakes of $M_w < 6$ in the northern Lesser
216 Antilles [López *et al.*, 2006] suggests some coupling of
217 the subduction interface there. Additional GPS sites are
218 needed in this region to better constrain the elastic strain
219 accumulation.

220 [14] The contribution of a coupled slab segment (or any
221 fault) to geodetic models falls off with distance from the
222 observations [Savage, 1983]. As the 1896 Sanriku and the
223 2011 Tohoku-Oki earthquakes have shown, strain accumu-
224 lation near the trench can result in significant earthquakes
225 and tsunamis [Simons *et al.*, 2011, and references therein].
226 To test whether convergent strain accumulation in the NE
227 Caribbean is not detected because of its distance from the
228 cGPS network, we applied trench-perpendicular conver-
229 gence in a 40-km-wide region closest to the trench. The
230 near-trench region with water depth of 7–8 km, was repre-
231 sented by 4 segments (yellow dashed rectangles N1–N4 in
232 Figure 1) with a dip of 6° and an up-dip and down-dip
233 depths of 8 and 12 km, respectively. The applied backslip is
234 proportional to the trench-perpendicular convergent plate
235 component of each segment (Table S3), and was multiplied
236 by a fraction between 0–1 to represent the magnitude of
237 locking. As before, the contributions of all 4 segments were
238 summed for each modeled site. The fit appears to decrease
239 with increasing fraction of inter-plate coupling (Figure 1f),
240 but the accumulation of up to 33% of the convergent plate
241 component near the trench ($<1.1, 1.1, 1.9,$ and 3.5 mm/y for
242 S1, S2, S3, and S4, respectively) cannot be rejected at
243 $\alpha = 0.05$. There have been several M 5–6 earthquakes north
244 of PRVI with very oblique thrust mechanisms (10° – 20°
245 from plate motion direction), mostly located closer to the
246 cGPS sites than to the trench [Doser *et al.*, 2005], but their
247 causes are presently unknown.

248 [15] Therefore, within the framework of our model
249 assumptions, the observed motion in Puerto Rico, the Virgin
250 Islands, and northern Lesser Antilles does not require trench-
251 perpendicular convergence although a small percentage of
252 locking close to the trench and in the forearc of the Lesser
253 Antilles cannot be rejected. The region north of Puerto Rico
254 may actually be extending slightly, as has been suggested by
255 Speed and Larue [1991].

4. Discussion

256 [16] Causes for the absence of subduction-directed motion,
257 particularly north of PRVI are further investigated below.
258 One possible cause is a coherent bias in the cGPS results,
259 perhaps due to inaccurate CA plate reference. However, this
260 is unlikely because multiple studies have yielded similar CA
261 Euler vectors (Table S2). Another possibility is that the cGPS
262 vectors represent a combination of trench-perpendicular
263 convergence and a much larger signal of regional rotation or
264 translation of the upper plate, as was deduced for the Cas-
265 cadia margin in Oregon [McCaffrey *et al.*, 2000]. Mann *et al.*
266 [2002] qualitatively proposed counter-clockwise (CCW)
267 rotation of PRVI around a hinge in Mona Passage, caused by
268 the collision of the Bahamas Platform with the Caribbean arc,
269 but could not determine if it continues today. Present-day
270 rotation of PRVI of the kind proposed by Mann *et al.* should
271

273 be expressed in the GPS data as an increase in the N com-
 274 ponent as a function of site distance eastward from Mona
 275 Passage. While a subset of the network (PUR5, P780, MIPR,
 276 ZSU1, and CUPR) shows such increase that can be inter-
 277 preted as CCW rotation around a pole at 67.10°W , 16.61°N
 278 ($\omega = 0.414 \pm 0.250 \text{ deg/m.y.}$), the trend becomes ambiguous
 279 when other sites are included (68.71°W , 12.65°N ,
 280 $\omega = 0.123 \pm 0.127 \text{ deg/m.y.}$) (Figure 1c). It could be argued
 281 that, as in Cascadia, the observed velocity is a combination of
 282 CCW rotation and trench-perpendicular convergence. To test
 283 this argument, we imposed on segments S1–S3 the trench-
 284 perpendicular convergent backslip from plate motion with
 285 30% locking. In such model, the N velocity due to CCW
 286 rotation is the difference between the observed and calculated
 287 N components. The trend remains ambiguous even when
 288 convergence is imposed (green dots in Figure 1c; 76.68°W ,
 289 16.73°N , $\omega = 0.044 \pm 0.052 \text{ deg/m.y.}$), suggesting that the
 290 NW velocity is not due to PRVI rotation.

291 [17] We suggest that plate divergence north of PRVI may
 292 result from slab retreat and or a tear in the slab [ten Brink,
 293 2005]. The maximum divergence (3 mm/y) is modeled in
 294 S2, where geological evidence for possible extension includes
 295 unusually deep ($>7500 \text{ m}$) forearc, very low (-380 mGal)
 296 free-air gravity anomaly, and a northward-tilting carbonate
 297 platform [ten Brink, 2005]. The carbonate platform was
 298 formed near sea level and is now up to 4000 m deep.

299 [18] We next focus the discussion on the trench parallel
 300 component of the cGPS data, which is generally larger than
 301 the trench-perpendicular component (compare Figures 1b
 302 and 1c). The magnitude of the trench-parallel component
 303 decreases with distance from the trench (Figure 1b) mim-
 304 icking the total vector magnitude. Negredo et al. [2004]
 305 suggested that an eastward asthenospheric flow at the base
 306 of the CA plate drags the plate eastward. van Benthem and
 307 Govers [2010] argued that the eastward motion is driven
 308 by suction force due to slab retreat of the Lesser Antilles
 309 subduction zone south of Guadeloupe. The eastward motion
 310 is resisted by friction on the plate boundaries [Negredo et al.,
 311 2004] or more specifically, by sticky points, such as the
 312 Bahamas Platform north of Hispaniola and a few volcanic
 313 ridges farther east [van Benthem and Govers, 2010]. This
 314 resistance creates a strong velocity gradient inward of the
 315 plate boundary, which in CA reference is expressed as
 316 decreasing westward velocity toward the plate interior
 317 (Figure 1b). If resistance along the NE Caribbean is provided
 318 mostly by the Bahamas platform [Mann et al., 2002], then
 319 PRVI could be dragged westward with Hispaniola only if
 320 the Greater Antilles oceanic island arc is rigid enough to
 321 transfer some of the force along the arc. The decreasing
 322 fraction of trench-parallel locking in the best-fit model from
 323 50% in western Puerto Rico to 0% north of the Virgin
 324 Islands may be representative of this westward drag. The
 325 large trench-parallel component of S4 is compatible with
 326 geological and seismological inferences for trench-parallel
 327 extensional deformation of the northern Lesser Antilles arc
 328 [Feuillet et al., 2002; López et al., 2006].

329 [19] Sites MOPR (Mona Island) and PRMI (SW Puerto
 330 Rico) move to the SW similar to GPS sites in Hispaniola,
 331 and unlike the NW-directed motion of the rest of the net-
 332 work (Figure 1) [López et al., 2011]. Velocities in Hispa-
 333 niola increase westward from values similar to our
 334 observations in Mona Passage, to $>10 \text{ mm/y}$ in central His-
 335 paniola [Calais et al., 2010]. Our suggested boundary

between Hispaniola and the PRVI, marked by heavy dashed
 red line in Figure 1, may extend north to Mona rift. The
 1918 Mw 7.2 [Doser et al., 2005] earthquake could have
 originated on this boundary. Abundant shallow seismicity in
 SW Puerto Rico shows mixed left-lateral strike slip and
 NNE-SSW extension [Huérffano et al., 2005]. The seismicity
 and active faults in SW Puerto Rico [Prentice and Mann,
 2005] and within Mona Passage (Figure 1) probably reflect
 NE-SW opening of Mona Passage [Chaytor and ten Brink,
 2010]. The relative motion across this boundary can be
 estimated from the difference in velocity between MOPR
 and PUR5 (1.9 mm/y in direction 220°) or between PRMI
 and P780 (3.1 mm/y in direction 241°) as SW-NE and not
 E-W as previously suggested [Jansma et al., 2000].

5. Conclusions

[20] It is difficult to reconcile NW-directed cGPS veloci-
 ties in Puerto Rico, Virgin Islands, and St. Maarten, with
 accumulation of trench-perpendicular thrust on a locked
 subduction interface, unless the locking percentage is low in
 the northern Lesser Antilles, and in the trench-proximal
 region north of PRVI. The data may in fact suggest that most
 of the interface north of PRVI is extending in agreement
 with abnormal bathymetry, gravity, and subsidence there.
 The trench-parallel component of the cGPS velocity decrea-
 ses gradually away from the trench, indicating an eastward
 motion of the interior CA plate relative to its northern
 boundary. Thus, if the cGPS data reflect the magnitude of
 coupling on the subduction interface, the subduction zone
 north of PRVI probably cannot generate mega-earthquakes,
 although damaging smaller earthquakes cannot be dis-
 counted. GPS velocity vectors in Mona Passage and SW
 Puerto Rico are directed southwestward relative to CA
 plate similar to GPS vectors in eastern Hispaniola and unlike
 those in PRVI, implying at least 2–3 mm/y of NE-SW
 extension across SW Puerto Rico and Mona Passage.

[21] **Acknowledgments.** We thank technicians from the Puerto Rico
 Seismic Network, and James Normandeau from UNAVCO for technical
 help with stations. Tim Dixon and Yan Jiang for technical help on GPS data
 processing, Andy Solow for help with the statistical analysis, and Brian
 Andrews, for help with Figure 1. Thoughtful reviews by Andrew Freed,
 Daniel Brothers, John Weber, and an anonymous reviewer are gratefully
 acknowledged.

[22] The Editor thanks John Weber and an anonymous reviewer for
 assisting with the evaluation of this paper.

References

- Atwater, B. F., U. S. ten Brink, M. Buckley, R. S. Halley, B. E. Jaffe, A. M.
 López-Venegas, E. G. Reinhardt, M. P. Tuttle, S. Watt, and Y. Wei
 (2012), Geomorphic and stratigraphic evidence for an unusual tsunami
 or storm a few centuries ago at Anegada, British Virgin Islands, *Nat.*
Hazards, doi:10.1007/s11069-010-9622-6, in press.
 Calais, E., A. Freed, G. Mattioli, F. Amelung, S. Jónsson, P. Jansma, S. H.
 Hong, T. Dixon, C. Prépetit, and R. Momplaisir (2010), Transpressional
 rupture of an unmapped fault during the 2010 Haiti earthquake, *Nat.*
Geosci., 3, 794–799, doi:10.1038/ngeo992.
 Chaytor, J. D., and U. S. ten Brink (2010), Extension in Mona Passage,
 northeast Caribbean, *Tectonophysics*, 493, 74–92, doi:10.1016/j.
 tecto.2010.07.002.
 DeMets, C., R. G. Gordon, and D. F. Argus (2010), Geologically current
 plate motions, *Geophys. J. Int.*, 181, 1–80, doi:10.1111/j.1365-
 246X.2009.04491.x.
 Dixon, T. H. (1993), GPS measurement of relative motion of the Cocos and
 Caribbean plates and strain accumulation across the Middle America
 trench, *Geophys. Res. Lett.*, 20, 2167–2170, doi:10.1029/93GL02415.
 Doser, D. I., C. M. Rodriguez, and C. Flores (2005), Historical earthquakes
 of the Puerto Rico-Virgin Islands region (1915–1963), in *Active*

- 401 *Tectonics and Seismic Hazards of Puerto Rico, the Virgin Islands, and*
 402 *Offshore Areas*, edited by P. Mann, *Spec. Pap. Geol. Soc. Am.*, 385,
 403 103–114.
- 404 Feuillet, N., I. Manighetti, P. Tapponnier, and E. Jacques (2002), Arc paral-
 405 lel extension and localization of volcanic complexes in Guadeloupe,
 406 Lesser Antilles, *J. Geophys. Res.*, 107(B12), 2331, doi:10.1029/
 407 2001JB000308.
- 408 Geist, E. L., and T. Parsons (2009), Assessment of source probabilities
 409 for potential tsunamis affecting the U.S. Atlantic coast, *Mar. Geol.*,
 410 264, 98–108, doi:10.1016/j.margeo.2008.08.005.
- 411 Hashimoto, C., A. Noda, T. Sagiya, and M. Matsu'ura (2009), Interplate
 412 seismogenic zones along the Kuril-Japan trench inferred from GPS data
 413 inversion, *Nat. Geosci.*, 2, 141–144, doi:10.1038/ngeo421.
- 414 Huérffano, V., C. von Hillebrandt-Andrade, and G. Baez-Sanchez (2005),
 415 Microseismic activity reveals two stress regimes in southwestern Puerto
 416 Rico, in *Active Tectonics and Seismic Hazards of Puerto Rico, the Virgin*
 417 *Islands, and Offshore Areas*, edited by P. Mann, *Spec. Pap. Geol. Soc.*
 418 *Am.*, 385, 81–101.
- 419 Jansma, P. E., and G. S. Mattioli (2005), GPS results from Puerto Rico and
 420 the Virgin Islands: Constraints on tectonic setting and rates of active
 421 faulting, in *Active Tectonics and Seismic Hazards of Puerto Rico, the Vir-*
 422 *gin Islands, and Offshore Areas*, edited by P. Mann, *Spec. Pap. Geol.*
 423 *Soc. Am.*, 385, 13–30.
- 424 Jansma, P. E., G. S. Mattioli, A. López, C. DeMets, T. H. Dixon, P. Mann,
 425 and E. Calais (2000), Neotectonics of Puerto Rico and the Virgin
 426 Islands, northeastern Caribbean, from GPS geodesy, *Tectonics*, 19,
 427 1021–1037, doi:10.1029/1999TC001170.
- 428 Lin, J., and R. S. Stein (2004), Stress triggering in thrust and subduction
 429 earthquakes and stress interaction between the southern San Andreas
 430 and nearby thrust and strike-slip faults, *J. Geophys. Res.*, 109, B02303,
 431 doi:10.1029/2003JB002607.
- 432 López, A. M., S. Stein, T. Dixon, G. Sella, E. Calais, P. Jansma, J. Weber,
 433 and P. LaFemina (2006), Is there a northern Lesser Antilles forearc
 434 block?, *Geophys. Res. Lett.*, 33, L07313, doi:10.1029/2005GL025293.
- 435 López, A. M., P. E. Jansma, G. S. Mattioli, S. A. James, D. Ihemedu, S. M.
 436 Quintana, and J. S. Salazar (2011), Constraining Puerto Rico-Virgin
 437 Islands microplate internal deformation with two decades of GPS
 438 observations, Abstract T23D-2450 presented at Fall Meeting, AGU,
 439 San Francisco, Calif., 5–9 Dec.
- 440 Manaker, D. M., E. Calais, A. M. Freed, S. T. Ali, P. Przybylski, G. Mattioli,
 441 P. Jansma, C. Pre'petit, and J. B. deChabaliér (2008), Interseismic plate
 442 coupling and strain partitioning in the northeastern Caribbean, *Geophys.*
 443 *J. Int.*, 174, 889–903, doi:10.1111/j.1365-246X.2008.03819.x.
- 444 Mann, P., E. Calais, J.-C. Ruegg, C. DeMets, P. E. Jansma, and G. S. Mattioli
 445 (2002), Oblique collision in the northeastern Caribbean from GPS measure-
 446 ments and geological observations, *Tectonics*, 21(6), 1057, doi:10.1029/
 447 2001TC001304.
- 448 McCaffrey, R., M. D. Long, C. Goldfinger, P. C. Zwick, J. L. Nabelek,
 449 C. K. Johnson, and C. Smith (2000), Rotation and plate locking at the
 southern Cascadia subduction zone, *Geophys. Res. Lett.*, 27, 3117–3120,
 doi:10.1029/2000GL011768.
- Negredo, A. M., I. Jiménez-Munt, and A. Villaseñor (2004), Evidence for
 eastward mantle flow beneath the Caribbean plate from neotectonic mod-
 eling, *Geophys. Res. Lett.*, 31, L06615, doi:10.1029/2003GL019315.
- Norabuena, E., L. Leffler-Griffin, A. Mao, T. Dixon, S. Stein, I. S. Sacks,
 L. Ocola, and M. Ellis (1998), Space geodetic observations of Nazca-
 South America convergence across the central Andes, *Science*, 279,
 358–362, doi:10.1126/science.279.5349.358.
- Prawirodirdjo, L., et al. (1997), Geodetic observations of interseismic strain
 segmentation at the Sumatra Subduction Zone, *Geophys. Res. Lett.*, 24(21),
 2601–2604, doi:10.1029/97GL52691.
- Prentice, C. S., and P. Mann (2005), Paleoseismic study of the South Lajas
 fault: First documentation of onshore Holocene fault in Puerto Rico, in
Active Tectonics and Seismic Hazards of Puerto Rico, the Virgin Islands,
and Offshore Areas, edited by P. Mann, *Spec. Pap. Geol. Soc. Am.*, 385,
 215–222.
- Savage, J. C. (1983), A dislocation model of strain accumulation and release
 at a subduction zone, *J. Geophys. Res.*, 88, 4984–4996, doi:10.1029/
 JB088iB06p04984.
- Simons, M., et al. (2011), The 2011 magnitude 9.0 Tohoku-Oki earthquake:
 Mosaicking the megathrust from seconds to centuries, *Science*, 332,
 1421–1425, doi:10.1126/science.1206731.
- Speed, R. C., and D. K. Larue (1991), Extension and transtension in the
 plate boundary zone of the northeastern Caribbean, *Geophys. Res. Lett.*,
 18, 573–576, doi:10.1029/91GL00394.
- ten Brink, U. (2005), Vertical motions of the Puerto Rico Trench and Puerto
 Rico and their cause, *J. Geophys. Res.*, 110, B06404, doi:10.1029/
 2004JB003459.
- ten Brink, U., W. H. Bakun, and C. H. Flores (2011), Historical perspective
 on seismic hazard to Hispaniola and the northeast Caribbean region,
J. Geophys. Res., 116, B12318, doi:10.1029/2011JB008497.
- Toda, S., R. S. Stein, K. Richards-Dinger, and S. B. Bozkurt (2005),
 Forecasting the evolution of seismicity in Southern California: Anima-
 tions built on earthquake stress transfer, *J. Geophys. Res.*, 110,
 B05S16, doi:10.1029/2004JB003415.
- van Benthem, S., and R. Govers (2010), The Caribbean plate: Pulled,
 pushed, or dragged?, *J. Geophys. Res.*, 115, B10409, doi:10.1029/
 2009JB006950.
- Westbrook, G. K., and W. R. McCann (1986), Subduction of Atlantic litho-
 sphere beneath the Caribbean, in *The Geology of North America*, vol. H,
The Caribbean Region, edited by G. Dengo and J. E. Case, pp. 341–350,
 Geol. Soc. of Am., Boulder, Colo.
- Zumberge, J. F., M. B. Heflin, D. C. Jefferson, M. M. Watkins, and F. H.
 Webb (1997), Precise point positioning for the efficient and robust
 analysis of GPS data from large networks, *J. Geophys. Res.*, 102(B3),
 5005–5017, doi:10.1029/96JB03860.